Journal of Assisted Reproduction and Genetics (2023) 40:1187–1195
https://doi.org/10.1007/s10815-023-02784-1

GAMETE BIOLOGY

Detection of spermatogonial stem/progenitor cells in prepubertal mouse testis with deep learning

Burak Kahveci[1] · Selin Önen[2,3] · Fuat Akal[4] · Petek Korkusuz[5]

Received: 7 November 2022 / Accepted: 21 March 2023 / Published online: 30 March 2023

Abstract

Purpose Rapid and easy detection of spermatogonial stem/progenitor cells (SSPCs) is crucial for clinicians dealing with male infertility caused by prepubertal testicular damage. Deep learning (DL) methods may offer visual tools for tracking SSPCs on testicular strips of prepubertal animal models. The purpose of this study is to detect and count the seminiferous tubules and SSPCs in newborn mouse testis sections using a DL method.

Methods Testicular sections of the C57BL/6-type newborn mice were obtained and enumerated. Odd-numbered sections were stained with hematoxylin and eosin (H&E), and even-numbered sections were immune labeled (IL) with SSPC specific marker, SALL4. Seminiferous tubule and SSPC datasets were created using odd-numbered sections. SALL4-labeled sections were used as positive control. The YOLO object detection model based on DL was used to detect seminiferous tubules and stem cells.

Results Test scores of the DL model in seminiferous tubules were obtained as 0.98 mAP, 0.93 precision, 0.96 recall, and 0.94 f1-score. The SSPC test scores were obtained as 0.88 mAP, 0.80 precision, 0.93 recall, and 0.82 f1-score.

Conclusion Seminiferous tubules and SSPCs on prepubertal testicles were detected with a high sensitivity by preventing human-induced errors. Thus, the first step was taken for a system that automates the detection and counting process of these cells in the infertility clinic.

Keywords Spermatogonial stem/progenitor cells · Testis · YOLO object detection · Deep learning · Computer vision

Introduction

The cancer treatments including chemo-radiotherapy applications result in permanent infertility in near to half of male childhood cancer survivors [1, 2]. Spermatogonial stem/progenitor cells (SSPC) are the only germ cell group in testes before puberty since the spermatogenesis is not initiated yet [3]. Because they constitute the only option for fertility preservation, there are several experimental methods developed for in vitro spermatogenesis or cryopreservation on testicular biopsies collected before gonadotoxic cancer treatment [1, 4, 5]. It is crucial to detecting and counting the number of SSCPs in testicular biopsy quickly by an automated method in order to determine further application on tissue or determining their therapeutic potential for infertility caused by testicular damage before puberty. Spermatogonial stem/progenitor cells are the pool of A_{single}, A_{paired}, and $A_{aligned}$ spermatogonia that reside on the basal membranes of seminiferous tubules and proliferated until puberty [6]. PLZF, THY-1, and SALL4 are the

✉ Petek Korkusuz
petek@hacettepe.edu.tr

Burak Kahveci
burakkahveci42@gmail.com

Selin Önen
selinonen@hacettepe.edu.tr

Fuat Akal
akal@hacettepe.edu.tr

1 Department of Bioengineering, Graduate School of Science and Engineering, Hacettepe University, Ankara, Turkey

2 Department of Stem Cell Sciences, Graduate School of Health Sciences, Hacettepe University, Ankara, Turkey

3 Department of Medical Biology, Faculty of Medicine, Atilim University, Ankara, Turkey

4 Computer Engineering Department, Hacettepe University, Ankara, Turkey

5 Department of Histology and Embryology, Faculty of Medicine, Hacettepe University, Sihhiye, 06100 Ankara, Turkey

specific markers of SSPCs and used in immunolabeling for detection of SSPC pool [7, 8]. To eliminate the quantification under microscope by human eye on immunolabeled sections might be beneficial for decreasing possible mistakes in laboratories. The preservation of the SSPCs presents the only tool for the cancer patients to open the road to have their biological children in the future. It is relatively easy to identify seminiferous tubules in a mouse testis section. However, SSPCs are found in low numbers within a complex niche environment with Sertoli cells that are morphologically significant and bigger sustentacular cells [9]. Consequently, it can be challenging, expensive, and prone to human error to detect SSPCs.

Artificial intelligence–based medical applications can be utilized in diagnosis and treatment protocols. These applications include data mining, medical expert systems, machine learning (ML), and image processing techniques [10–12]. There are several studies in the literature focused mainly on seminiferous tubules, multi-site segmentation, and multiple cell segmentation [13–16], different types of segmentation, and automatized classification models for staging H&E-stained seminiferous tubules on mouse [13, 14, 17], rat [16], and human [18, 19] testicular sections. A DL model provided the classification of normal and abnormal mouse seminiferous tubules at 98% accuracy [15]. Neural network-based automatized systems demonstrated varying accuracy on detecting sperm morphology classification [20], segmentation of internal and external parts of sperms [21], and detection and analysis of different parts of human sperms [22].

Several DL techniques provided high accuracy for detection of spermatogenic cells in seminiferous tubules of adult rodent models and also human samples (Table 1). However, prepubertal testicular tissues where the spermatogenesis has not been initiated yet are not examined by using AI that would contribute to an efficient tool for detection and quantification of germ stem cells in cancer patients to diagnose and treat male infertility. In this study, we hypothesized to develop a bioengineering system that allows the detection of seminiferous tubules and rapid, safe, and easy quantification of SSPCs by using DL. To test the hypothesis, we obtained, digitized, and labeled paraffin sections from C57BL/6 neonatal male mice testes and built DL models. Our study demonstrated promising results to prevent human-induced errors while providing high sensitivity and rapid detection of seminiferous tubules and SSPCs.

Methods

Experimental design

The study is planned as an observational, interdisciplinary, experimental study. Dependent variables are SSPC and seminiferous tubule numbers; independent variables are manual counts and AI-based image analysis outputs related to SSPCs and seminiferous tubules. All experiments were carried out on sections obtained from testicular blocks of 3 newborn C57BL/6 male mice (6 testes), which was used within the scope of Hacettepe University Animal Experiments Local

Table 1 The applications of DL methods in reproductive system tissues and cells

Dataset	Goals	Methods	Results	Ref
Mouse testis	Seminiferous tubules classification	• SAE with hyperlayer	Accuracy: 98%	[15]
	Seminiferous tubules segmentation Multi-cell segmentation Multi-region segmentation	• ResNet • FCNN	Accuracy: 94.40%, 91.26%, 93.47%	[13]
	Seminiferous tubules segmentation Spermatogenic cells and multi-concentric-layer segmentation	• ResNet • U-Net	Accuracy: 91.20%, 92.95%, 91.08%	[14]
	Seminiferous tubules segmentation Multi-cell segmentation	• SED-Net	Pixel accuracy: 93.0%, intersection over union: 87.8%	[17]
Rat testis	Identifying spermatogenic stages in seminiferous tubules	• U-Net	Accuracy: 98.4%	[16]
Human testis	Determining Johnsen scoring using AI	• ANN	Precision, 96.29%	[18]
	Automatic annotation of IHC images	• HBNN	mAP, 76.0%	[19]
Sperm	Classification	• CNN	Accuracy: 94%	[20]
	Segmentation of internal and external parts of sperm	• CNN • K-means	Dice similarity coefficient: 90.4% (head), 77.3% (acrosome), 78.8% (nucleus)	[21]
	Detection and analysis of different parts of human sperms	• CNN	Accuracy: 76.77% (acrosome), 77% (head), 91.33% (vacuole)	[22]

Ethics Committee document dated 04.09.2018 and numbered 52338575-96 received for the project number TYL-2018-17531. The program codes used in this study can be accessed from the GitHub repository.

Histological techniques

Testes obtained from C57BL/6-type neonatal mice were fixed by immersion in Bouin's fixative, dehydrated in graded series of ethanol cleared in xylene in a vacuum tissue processor (Leica, Germany) and embedded in paraffin in embedding station (Leica, Germany). Serial sections of 3-µm thickness were taken in the sliding microtome (Leica, Germany). The sections were deparaffinized in the drying oven at 60 °C overnight and then rehydrated with a graded series of alcohols. Consecutive serial sections were stained with H&E [4] or IL for SSPCs. For immune labeling briefly [23], heat-induced antigen retrieval method was applied in a pressure cooker within the citrate buffer solution (pH = 6.5) (Abcam, USA) for 5–10 min. After the sections were washed, a protein block was performed with goat serum at room temperature for 10 min (Abcam, USA). The sections were incubated with rat anti-mouse SALL4 (ab29112, Abcam, UK) primary antibody at 1:200 dilution for 15–30 min at RT in humidity chamber. DAB chromogen was applied to sections that were incubated for 15 min with goat anti-rat IgG-HRP-conjugated secondary antibody (Abcam, USA) at room temperature. After the DAB chromogen was dropped, the labeling was followed under the bright field microscope for 5–7 min. Tissues, which were not treated with primary antibody, were used as negative control. Nuclear staining was performed with hematoxylin for 30 s. Sections were washed with phosphate buffer saline (pH: 7.4), dehydrated with graded alcohols, and coverslipped by using an entellan mounting medium (Merck, USA).

Dataset preparation

Testis micrographs were obtained by using a light microscope with a digital camera attachment (Leica DM 6000 DM, Germany). These micrographs were digitized using the image analysis system (LASv3 Leica, Germany) with 3264 × 2448 and 1920 × 1940 resolutions.

Two datasets, namely the seminiferous tubule dataset and the SSPCs dataset, were created with these micrographs to use in this study. Accurately identifying the quantity of SSPCs by using H&E-stained micrographs only is not viable. Therefore, to identify SSPCs on an H&E-stained micrograph, we referred to the IL micrograph that corresponds to the same region on the consecutive section and expected that the two sections are quite similar. Note that we labeled only the H&E-stained micrographs for both seminiferous tubules and SSPCs to create our datasets. We obtained consecutive sections from different blocks and enumerated them block-wise. The odd-numbered sections were stained with H&E, while the even-numbered ones were IL. For instance, when we obtained six sections from a block, sections were enumerated from 1 to 6. After having stained or IL the section, we had six consecutive sections as 1:H&E → 2:IL → 3:H&E → 4:IL → 5:H&E → 6:IL. In this example, labeling of H&E-stained sections 1, 3, and 5 was done by using immune-labeled sections 2, 4, and 6, respectively. In total, we had 35 odd-numbered and 20 even-numbered sections to use for creating the labeled seminiferous tubule and the SSPCs datasets, respectively. In case the immune labeling of section 4 does not produce desired results and cannot be used to label section 3, section 2 is used to label section 3. That is, we are using section 2 to label both sections 1 and 3. This makes the method fault tolerant. That means, we can still label H&E-stained sections even though, at most, half the immune labeling fails.

For the seminiferous tubule dataset, 909 micrographs were obtained from 35 sections. The total size of these micrographs was 10.3 gigabytes. For the SSPC dataset, 1114 micrographs were obtained from 20 sections. The total size of these micrographs was 11.5 gigabytes. The micrographs were resized (416 × 416) and labeled with the Labellmg program [24].

Deep learning method

Seminiferous tubules and SSPCs were detected with the YOLOv5 object detection model using photos with 3264 × 2448 and 1920 × 1940 pixel dimensions, respectively. All photos were obtained with 630 × magnification. The YOLO model was created using the Python programming language and trained on the Google Cloud.

Figure 1 shows the workflow used to detect seminiferous tubules. Sections from C57BL/6-type newborn mice were stained with H&E (Fig. 1a). Micrographs with 3264 × 2448 and 1920 × 1940 resolutions were obtained from these sections by using a light microscope (Fig. 1b). These micrographs constitute the raw dataset. Tubules on these raw images were labeled with the LabelImg program to prepare the dataset to be used in evaluations (Fig. 1c). The labeled dataset is split into train and test sets by using an 80/20% split ratio, and, to further increase the size and diversity of the dataset, data augmentation was applied to the training data by using the Roboflow application [25]. The data augmentation process includes flip, 90- and 45° rotation, 50% crop, 50% grayscale, 25% brightness enhancement, 40% saturation, and mosaic actions. After the augmentation, a dataset consisting of 14,092 images was obtained. The dataset's size was 484 megabytes in total. Then, a YOLO object detection model was trained and tested (Fig. 1d). Finally, the detection of the seminiferous tubules was performed, and the results were obtained (Fig. 1e).

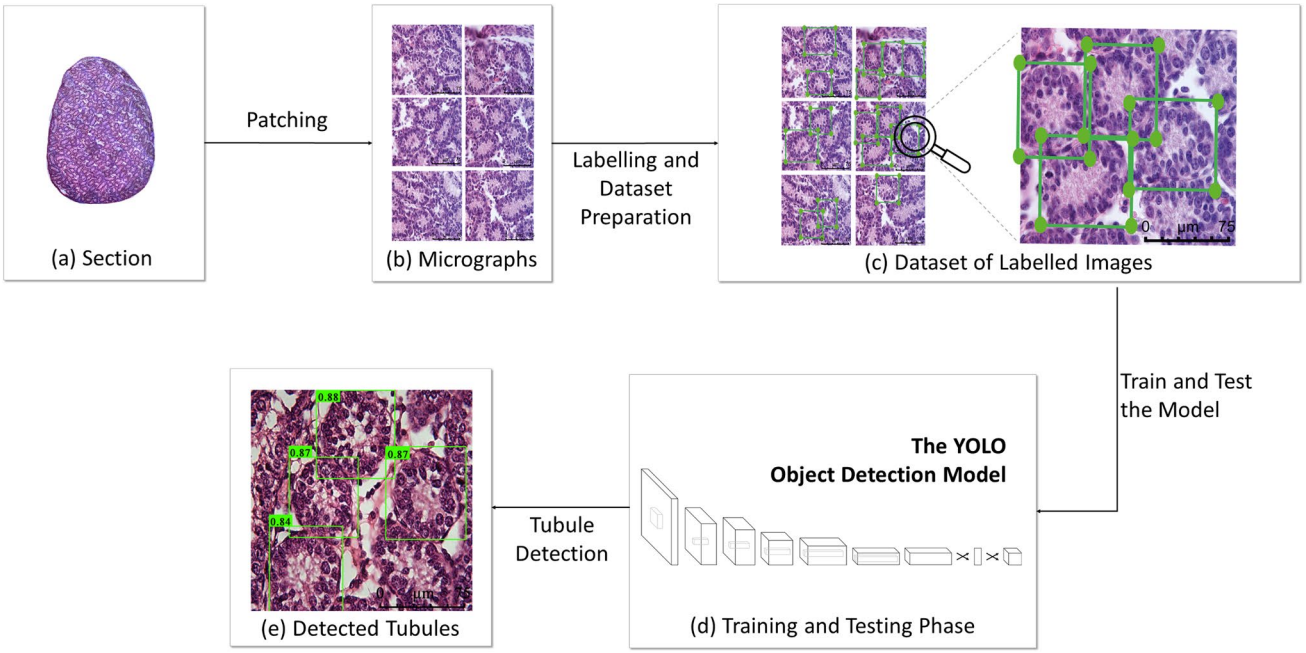

Fig. 1 The detection process of seminiferous tubules. **a** C57BL/6-type neonatal male mice testes sections. **b** Patches were obtained from sections by light microscopy. **c** Seminiferous tubules with an average width of 55 µm and a height of 58 µm were labeled with the LabelImg program, and a labeled dataset was created. **d** A DL model was trained and tested. **e** Detected seminiferous tubules on micrographs were shown

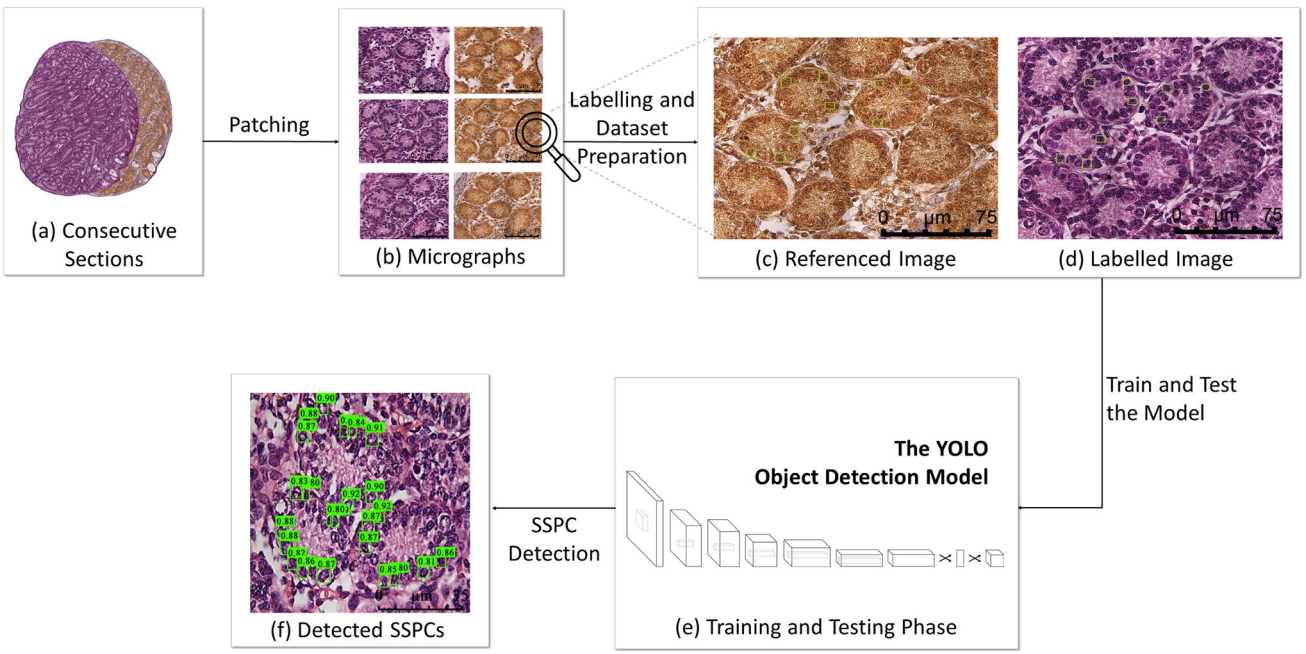

Fig. 2 The detection process of SSPCs. **a** C57BL/6-type neonatal male mice testes consecutive sections. **b** Patches were obtained from sections by light microscopy. **c**, **d** Spermatogonial stem/progenitor cells were labeled on H&E-stained sections by referencing immunolabeled serial sections. Labeling was done using the LabelImg program, and a prepared dataset was created. **e** Training and testing phases were applied in the DL method using the training and test datasets. **f** Detected SSPCs on micrographs were shown

Figure 2 shows the workflow used to detect SSPCs. Sections from C57BL/6-type newborn mice were either stained with H&E or IL. More concretely, once a section was H&E stained, its consecutive section was IL (Fig. 2a). Micrographs with 3264 × 2448 and 1920 × 1940 resolutions were obtained from these sections by light microscope (Fig. 2b). SSPCs in H&E-stained micrographs were identified by referencing the immune-labeled micrographs (Fig. 2c) and then labeled using the LabelImg program to obtain the prepared dataset (Fig. 2d). The labeled dataset is split into train and test sets by using a 60/40% split ratio, and, to further increase the size and diversity of the dataset, data augmentation was applied to the training data similar to the seminiferous tubule dataset. After the augmentation, the SSPCs dataset consisted of 13,964 micrographs and was 415 megabytes. Then, a YOLO object detection model was trained and tested (Fig. 2e). The experiment has been initiated by manually counting and labeling of SSPCs on H&E-stained sections in accordance with SALL4 immune labeling and further subsequent comparison of outputs of all the manual counting with that of our novel DL-based detection system. The obtained accuracy percentage (mAP success rate) of the developed DL model (Fig. 2f) is completely based on a sequential comparison of detected cells by system with manually labeled cells by experts.

Table 2 Test scores for seminiferous tubule detection

Seminiferous tubule detection test scores			
mAP	Recall	Precision	F1-Score
0.98	0.96	0.93	0.94

Results

Detection of seminiferous tubules

To detect seminiferous tubules, a DL model was trained with the labeled seminiferous tubule dataset. A threshold value of 65% was determined for the optimum plotting of the determinations. The detection process was completed in 5 iterations. The final mAP (mean average precision) score was 98%. Then, we tested our DL model with the labeled test dataset. We considered four metrics in our tests, namely mAP, recall, precision and f1-scores. The results are presented in Table 2. We obtained 0.98 mAP, 0.93 precision, 0.96 recall, and 0.94 f1-score as results from our tests.

Some examples regarding seminiferous tubule detection are shown in Figs. 3 and 4. The detected tubules are marked with boxes that surround them. Numerical values given on top of the boxes show the mAP scores of the detection. Figure 3 shows some examples on which all suitable seminiferous tubules were detected correctly.

Occasionally, a part of a seminiferous tubule may not be seen on the micrograph. Yet, it is detected by the DL model. Examples of such tubules are marked with white stars on Fig. 4a. The DL model we use tends to recognize objects in principle. Therefore, the model somehow completes the circular shape and returns a correctly detected tubule. Unfortunately, our model was not able to detect a small number of tubules on some micrographs. To our understanding, a suitable seminiferous tubule should be nearly round shape circular, has clear borders, and at a specific size (56 µm width, 58 µm height). We do not expect to detect tubules that do not fit in this description. In Fig. 4, we also show such a seminiferous tubule within boxes drawn with white dashed lines. Failure to detect a seminiferous tubule may have occurred due to their shape

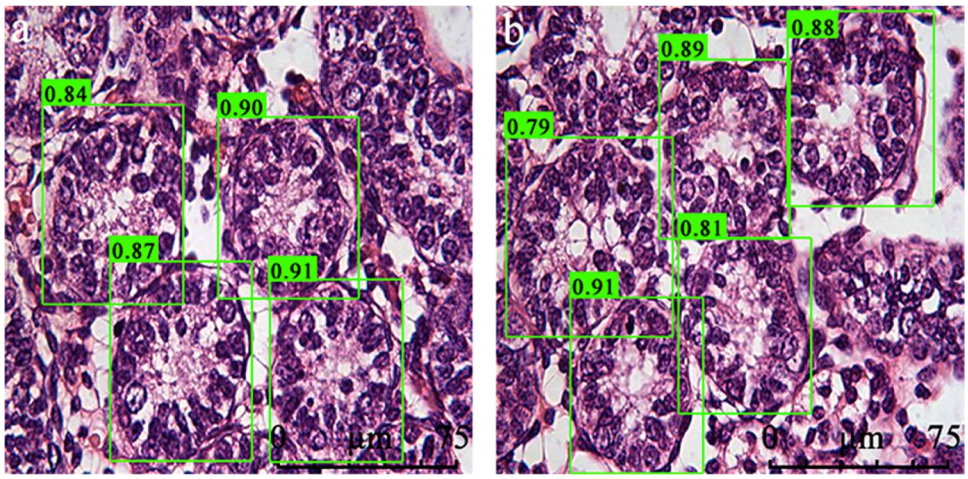

Fig. 3 Examples of micrographs on which all suitable seminiferous tubules were identified by the model were given. **a**, **b** × 630, H&E

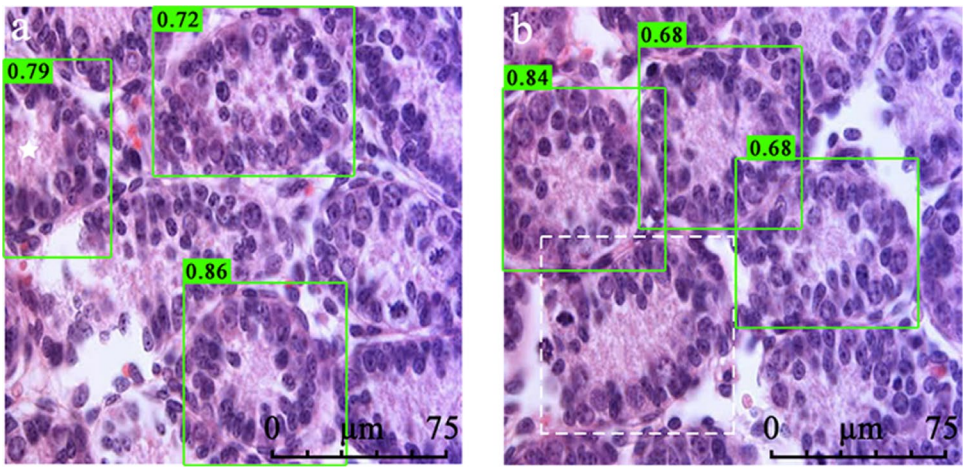

Fig. 4 A seminiferous tubule, which is detected in half in the micrograph and cannot be detected when it should be detected, is shown. **a** Half seminiferous tubule marked with a white star detected with a mAP of 0.79 on the left side of the micrograph. **b** Seminiferous tubule that cannot be detected on micrograph is marked with a dashed line because its border is uncertain. **a**, **b** × 630, H&E

Table 3 Test scores for SSPC detection

SSPC detection test scores			
mAP	Recall	Precision	F-1 score
0.88	0.83	0.80	0.82

and size. For example, a seminiferous tubule in Fig. 4b may have been missed due to its unclear borders.

Detection of spermatogonial stem/progenitor cells

To detect SSPCs, a DL model was trained with the labeled SSPC dataset. A threshold value of 65% was determined for the optimum plotting of the determinations. The detection process was completed in 109 iterations. The final mAP (mean average precision) score was 88%. Then, we tested our DL model with the labeled test dataset. In SSPC detection, we considered four metrics in our tests, namely mAP, recall, precision, and f1-scores. The results are seen in Table 3. We obtained 0.88 mAP, 0.80 precision, 0.83 recall, and 0.82 f1-score as results from our tests.

The detected cells are marked with boxes that surround them as seen in Fig. 5. Numerical values given on top of the boxes show the mAP scores of the detection.

Discussion

The spermatogenesis cycle, which proceeds similarly in rodents and humans, is a process that starts with spermatogonial stem cells and ends with spermatozoa and is regulated by many different gene expressions [26]. We used neonatal mice as animal models in this study. This system might provide a solution for rapid determination of fertility status of prepubertal cancer patients when used in humans. In our study, sections were obtained by staining C57BL/6-type neonatal mouse testis containing A, In and B spermatogonia (early stage including stages I–IV) with H&E, and datasets were created. Deep learning models were trained using seminiferous tubules and immune-labeled SSPC datasets. They are used to detect seminiferous tubules and SSPCs in H&E-stained sections. The seminiferous tubule dataset was created with micrographs

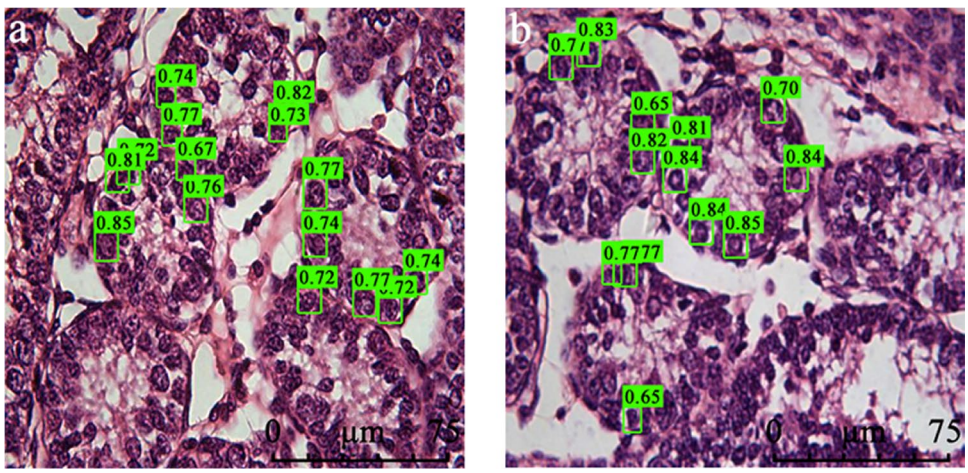

Fig. 5 Sample micrographs with SSPCs detected by the model are given. **a**, **b** × 630, H&E

obtained from 35 and 14,092 images. The DL model detected seminiferous tubules with a 98% mAP score. The SSPC dataset was created with 20 sections and 13,964 images. The model detected stem cells with an 88% mAP score.

There are several AI studies that we can directly compare with our work [13–17]. Kao and McMillan classified seminiferous tubules from mouse testis sections using stacked autoencoders [15]. In the study, sections were stained with H&E. The dataset consisted of 10,542 tubule image patches, and they achieved 98% classification accuracy. Xu et al. used ResNet and a fully convolutional neural network for seminiferous tubule, multi-cell and multi-zone segmentation to determine spermatogenesis staging on H&E-stained sections in 28 mice [13]. The ResNet model achieved accuracy scores of 94.40% and 91.26% for seminiferous tubule segmentation and multi-cell segmentation including SSPCs, respectively. Xu et al. used ResNet and U-net to perform seminiferous tubule and spermatogenic cell segmentation by using H&E-stained 40 adult mouse testis sections in another study [14]. They achieved accuracy scores of 91.20% and 92.95%, respectively. Liang et al. developed a tubule and multi-cell segmentation model using two separate datasets created from mouse testis sections [17]. They used 12 slices for datasets for the segmentation of tubules, spermatocytes, spermatogonia, round spermatids, and Sertoli cells. Their DL model was able to segment with 93% mean pixel accuracy. Creasy et al. used U-Net to determine spermatogenic stages of H&E-stained testis sections obtained from rats at different ages [16]. They achieved 98.4% accuracy. Sziva et al. performed a mathematically based histomorphometric image analysis study on images obtained from 22 different 4-week-old rat testis sections with different vitamin D levels induced [27]. They used H&E and immunohistochemically stained slides from paraffin-embedded sections in this study. With this model used, they detected the seminiferous tubules in the sections. They also detected seminiferous tubules containing elongated spermatids. They observed the receptor expressions in the sections where immunochemical staining was performed. The model used in this study is mathematically based and not an AI-based approach as in our study. In addition, the study focused on the detection of seminiferous tubule and seminiferous tubule sections, and SSPCs were not detected as in our study. Detection of seminiferous tubules containing only elongated spermatids may be similar to our study. However, in our study, we presented a more complete approach by detecting both seminiferous tubule and SSPCs with the innovative DL model, YOLO.

When the number of sections used and the accuracy rates obtained from the experiments are compared, our study presents similar values and characteristics to those in the literature [13–17]. However, our main contribution is twofold. First, our study uses mouse testis sections only in the early stages (stages I–V) of spermatogenesis. This makes the detection of SSPCs especially hard due to the underdeveloped forms of the cells. In this study, neonatal mice simulate prepubertal cancer patients. In children, the biopsy that can be taken is in lower amount than adults since their testicular size and the morbidity of the surgical procedure are higher. Therefore, the success, accuracy, reliability, and especially the quick response of the system are very important for translation to clinical use in prepubertal patients. When we look at the related work, they typically work with the cells from mid-stages (stages VI–VIII). Some studies [16, 17] try to find a balance and to classify early stages as well. However, their dataset, i.e., sections contain mostly the mid-stage sections; for instance, roughly 40% and 42% of the used sections from early stages of the spermatogenesis in [16] and [17], respectively. Liang et al. leaves annotating cell types in the early stages to a future work [17]. Second, to the best of our knowledge, our study is the first to use an object detection model to identify cells or tubules while all other related works use segmentation models. There are several practical advantages of the object detection model over segmentation. First, labeling images is relatively easy as it involves only drawing boxes, while this task may be as tedious as drawing an amorphous region in segmentation. Second, the YOLO object detection model we used is proved to be a faster method [28]. Third, the object detection model may complete circular shapes that are not seen well in an image and return a correctly detected tubule.

The study has several limitations. The DL model we used to detect SSPCs is 10–16% less effective on average as compared to seminiferous tubule detection. Due to the nature of the prepubertal organ structure, there are small number of SSPCs in newborn-mice testicular samples used. On the other hand, our findings are reliable since the statistical relevance and parametric distribution of the samples were confirmed and our data is accurate on a challenging small amount of testicular tissue that presents only scarcely distributed, small amount of stem cells as target object. Also, our results are limited to an animal model, which cannot accurately make exact simulation of human conditions since our assay does not contain any human testicular sample due to ethical reasons. The size and content of SSPC subpopulations have some differences in mice and humans. The proportion of SSCs to SSPCs and to total germ cells is lower in mice when compared to humans. The undifferentiated spermatogonia (A_{single}, A_{paired}, $A_{aligned}$) makes up 0.3% of germ cells in mice; however, in humans, the proportion of undifferentiated cells (A_{pale}, A_{dark}) reaches up to 22% [29] . Since the cellular morphology differs in the subpopulations, the accuracy of the newly generated DL-based detection system should further be tested in testicular sections of human prepubertal male cancer patients. On the other hand, because the testicular anatomy and tubular morphology of prepubertal humans and mice are similar as having a tortuous structure, containing Sertoli cells and SSPCs lying on basement membrane in tubules, our DL model is likely be suitable for use in human samples. The

study is limited to identification of seminiferous tubules and SSPCs. Thus, we did not include the identification of Sertoli cells. Sertoli cells are clearly distinguished in both H&E-stained and SALL4-immune-labeled seminiferous tubule sections from the small rounded SSPCs with their pyramidal morphology and huge size [30]. The smaller-sized germ cells consist of SSPCs only at this neonatal stage [9], lying on the basement membrane adjacent to or penetrating on the recesses of giant sustentacular Sertoli cells. Since the detection of the SSPCs that are harmed in cancer therapies was aimed, we did not need to include extra Sertoli cell labeling and quantification in our training set-up.

We have performed a preliminary study with a high percentage of accuracy with the SSPC dataset validated by immunohistochemistry. Our study aimed at detecting the testicular seminiferous tubules and SSPCs in prepubertal mice tissues, and we obtained 98% mAP in the detection of seminiferous tubules and 88% mAP in the detection of SSPCs. Some studies differentiate epithelial and stromal regions of human ovarian tissue and classify ovarian cancer using CNN [31, 32]. In these studies, H&E-stained sections were used, and 90.2% and 78.29% accuracy rates were obtained, respectively. CNN was used in studies where the classification and morphological analysis of sperms were made [20–22]. A 94% accuracy rate was obtained from the sperm classification study [20]. In the study in which sperms acrosomes, heads, and vacuoles were classified, the accuracy rates were 76.77%, 77%, and 91.33%, respectively [22]. In the study where the internal and external parts of the sperm were segmented, 90.4%, 77.3%, and 78.8% dice similarity coefficients were obtained for the head, acrosome, and nucleus, respectively [21]. In the study by Ito et al., a DL model was created for Johnsen score classification. While 82.6% precision value was obtained with × 400 magnification images, 99.5% precision value was obtained with expansion image dataset. In the study, H&E-stained human testis tissue sections were used [18]. In the study for automatic detection of different cell types on immunohistochemistry images, human testis cross-section images were used, and the trained model achieved a confidence score of 96.3% [19]. In these studies, using human tissues and cells close to testicular tissue, similar rates were obtained with the mAP rates we obtained in the detection of seminiferous tubules and SSPCs. Thus, we were able to academically validate the usability of the AI system in testicular tissues and germ stem/progenitor cells.

Conclusion

Spermatogonial stem/progenitor cells are few in number and difficult to detect. In this paper, the detection of seminiferous tubules and SSPCs with high sensitivity in 6-day-old mouse testis sections using the DL model was performed.

Our contribution has three facets. First, we created a labeled dataset of mouse testis sections, which we could use for further research. Second, we detected SSPCs on H&E-stained images with high sensitivity and removed the SALL4 marking step from the workflow, which is expensive and requires time and expertise. Third, we proved that SSPC detection can be automated, and human-induced errors in manual counting can be prevented. This automated AI-based SSPC content assessment method might be inserted in certain checkpoints before and/or after cryopreservation of biopsied testicular tissue from patients in clinics. And the evaluation results may shape the further application to the tissue including in vitro culture for increasing the pool of SSPCs or direct transplantation at adult ages after the gonadotoxic treatment finishes.

Author contribution Burak Kahveci and Petek Korkusuz generated the hypothesis. Sections were taken by Selin Önen and Burak Kahveci. Selin Önen guided and they both performed the histochemical and immunohistochemical staining. Burak Kahveci created the datasets. Burak Kahveci and Fuat Akal created the DL models and carried out the experiments. Petek Korkusuz and Fuat Akal edited the manuscript. All the authors read and approved the manuscript.

Funding This work was financially supported by Hacettepe University Scientific Research Project Coordination Unit; the (#TYL-2019-18375) TUBİTAK (The Scientific and Technological Research Council of Turkey) 1001 program supported Burak Kahveci as a scholar (#218S421).

Code availability https://github.com/burakkahveci/Detection-of-Spermatogonial-Stem-Cells.

Declarations

Ethics approval Animal materials used in the experiments were approved by Hacettepe University Animal Experiments Local Ethics Committee (#2018, 52338575-96).

Consent to participate Not applicable .

Consent for publication Not applicable .

Conflict of interest The authors declare no competing interests.

References

1. Skaznik-Wikiel ME, Gilbert SB, Meacham RB, Kondapalli LA. Fertility preservation options for men and women with cancer. Rev Urol. 2015;17(4):211–9. https://doi.org/10.3909/riu0666.
2. Wasilewski-Masker K, Seidel KD, Leisenring W, Mertens AC, Shnorhavorian M, Ritenour CW, Stovall M, Green DM, Sklar CA, Armstrong GT, Robison LL, Meacham LR. Male infertility in long-term survivors of pediatric cancer: a report from the childhood cancer survivor study. J Cancer Surviv. 2014;8(3):437–47. https://doi.org/10.1007/s11764-014-0354-6.
3. Levine JM. Preserving fertility in children and adolescents with cancer. Children. 2014;1(2):166–85. https://doi.org/10.3390/children1020166.
4. Önen S, Köse S, Yersal N, Korkusuz P. Mesenchymal stem cells promote spermatogonial stem/progenitor cell pool and spermatogenesis

in neonatal mice in vitro. Sci Rep. 2022;12(1):11494. https://doi.org/10.1038/s41598-022-15358-5.
5. Yersal N, Köse S, Horzum U, Özkavukcu S, Orwig KE, Korkusuz P. Leptin promotes proliferation of neonatal mouse stem/progenitor spermatogonia. J Assist Reprod Genet. 2020;37(11):2825–38. https://doi.org/10.1007/s10815-020-01929-w.
6. Kubota H, Brinster RL. Spermatogonial stem cells. Biol Reprod. 2018;99(1):52–74. https://doi.org/10.1093/biolre/ioy077.
7. Lovelace DL, Gao Z, Mutoji K, Song YC, Ruan J, Hermann BP. The regulatory repertoire of PLZF and SALL4 in undifferentiated spermatogonia. Development. 2016;143(11):1893–906. https://doi.org/10.1242/dev.132761.
8. Korkusuz P, Köse S, Yersal N, Önen S. Magnetic-based cell isolation technique for the selection of stem cells. Methods Mol Biol. 2019;1879:153–63. https://doi.org/10.1007/7651_2018_151.
9. Köse S, Yersal N, Önen S, Korkusuz P. Comparison of hematopoietic and spermatogonial stem cell niches from the regenerative medicine aspect. Adv Exp Med Biol. 2018;1107:15–40. https://doi.org/10.1007/5584_2018_217.
10. Amisha, Malik P, Pathania M, Rathaur V. Overview of artificial intelligence in medicine. J Family Med Primary Care. 2019;8(7):2328–31. https://doi.org/10.4103/jfmpc.jfmpc_440_19.
11. Louis CM, Erwin A, Handayani N, Polim AA, Boediono A, Sini I. Review of computer vision application in in vitro fertilization: the application of deep learning-based computer vision technology in the world of IVF. J Assist Reprod Genet. 2021. https://doi.org/10.1007/s10815-021-02123-2.
12. Chan YK, Chen YF, Pham T, Chang WD, Hsieh MY. Artificial intelligence in medical applications. J Healthc Eng. 2018:2. https://doi.org/10.1155/2018/4827875.
13. Xu J, Lu H, Li H, Wang X, Madabhushi A, Xu Y. Histopathological image analysis on mouse testes for automated staging of mouse seminiferous tubule. Cham: Springer International Publishing; 2019. https://doi.org/10.1007/978-3-030-23937-4_14.
14. Xu J, Lu H, Li H, Yan C, Wang X, Zang M, Rooij DG, Madabhushi A, Xu EY. Computerized spermatogenesis staging (CSS) of mouse testis sections via quantitative histomorphological analysis. Med Image Anal. 2021;70:101835. https://doi.org/10.1016/j.media.2020.101835.
15. Kao C-Y, McMillan L. A novel deep learning architecture for testis histology image classification. arXiv preprint arXiv:1707.05809; 2017. https://doi.org/10.48550/arXiv.1707.05809.
16. Creasy DM, Panchal ST, Garg R, Samanta P. Deep learning-based spermatogenic staging assessment for hematoxylin and eosin-stained sections of rat testes. Toxicol Pathol. 2021;49(4):872–87. https://doi.org/10.1177/0192623320969678.
17. Liang S, Lu H, Zang M, Wang X, Jiao Y, Zhao T, Xu EY, Xu J. Deep SED-Net with interactive learning for multiple testicular cell types segmentation and cell composition analysis in mouse seminiferous tubules. Cytometry A. 2022. https://doi.org/10.1002/cyto.a.24556.
18. Ito Y, Unagami M, Yamabe F, Mitsui Y, Nakajima K, Nagao K, Kobayashi H. A method for utilizing automated machine learning for histopathological classification of testis based on Johnsen scores. Sci Rep. 2021;11(1):9962. https://doi.org/10.1038/s41598-021-89369-z.
19. Ghoshal B, Hikmet F, Pineau C, Tucker A, Lindskog C. DeepHistoClass: a novel strategy for confident classification of immunohistochemistry images using deep learning. Mol Cell Proteomics. 2021;20:100140. https://doi.org/10.1016/j.mcpro.2021.100140.
20. Riordon J, McCallum C, Sinton D. Deep learning for the classification of human sperm. Comput Biol Med. 2019;111:103342. https://doi.org/10.1016/j.compbiomed.2019.103342.
21. Movahed RA, Mohammadi E, Orooji M. Automatic segmentation of sperm's parts in microscopic images of human semen smears using concatenated learning approaches. Comput Biol Med. 2019;109:242–53. https://doi.org/10.1016/j.compbiomed.2019.04.032.
22. Javadi S, Mirroshandel SA. A novel deep learning method for automatic assessment of human sperm images. Comput Biol Med. 2019;109:182–94. https://doi.org/10.1016/j.compbiomed.2019.04.030.
23. Bilgic E, Guzel E, Kose S, Aydin MC, Karaismailoglu E, Akar I, Usubutun A, Korkusuz P. Endocannabinoids modulate apoptosis in endometriosis and adenomyosis. Acta Histochem. 2017;119(5):523–32. https://doi.org/10.1016/j.acthis.2017.05.005.
24. Tzutalin, LabelImg. 2015. https://github.com/tzutalin/labelImg.
25. Roboflow. *Roboflow.* 2020; https://roboflow.com/about.
26. Ibtisham F, Wu J, Xiao M, An L, Banker Z, Nawab A, Zhao Y, Li G. Progress and future prospect of in vitro spermatogenesis. Oncotarget. 2017;8(39):66709–27. https://doi.org/10.18632/oncotarget.19640.
27. Sziva RE, Ács J, Tőkés AM, Korsós-Novák Á, Nádasy GL, Ács N, Horváth PG, Szabó A, Ke H, Horváth EM, Kopa Z, Várbíró S. Accurate quantitative histomorphometric-mathematical image analysis methodology of rodent testicular tissue and its possible future research perspectives in andrology and reproductive medicine. Life. 2022;12(2). https://doi.org/10.3390/life12020189.
28. Redmon J, Divvala S, Girshick R, Farhadi A. You only look once: unified, real-time object detection. In: Proceed IEEE Conference Comput Vision Pattern Recognition; 2016. https://doi.org/10.1109/CVPR.2016.91.
29. Fayomi AP, Orwig KE. Spermatogonial stem cells and spermatogenesis in mice, monkeys and men. Stem Cell Res. 2018;29:207–14. https://doi.org/10.1016/j.scr.2018.04.009.
30. Silber S. Histology of the testis and spermatogenesis. In: Silber S, editor. Fundamentals of Male Infertility. Cham: Springer International Publishing; 2018. p. 29–37. https://doi.org/10.1007/978-3-319-76523-5.
31. Du Y, Zhang R, Zargari A, Thai TC, Gunderson CC, Moxley KM, Liu H, Zheng B, Qiu Y. Classification of tumor epithelium and stroma by exploiting image features learned by deep convolutional neural networks. Ann Biomed Eng. 2018;46(12):1988–99. https://doi.org/10.1007/s10439-018-2095-6.
32. Wu M, Yan C, Liu H, Liu Q. Automatic classification of ovarian cancer types from cytological images using deep convolutional neural networks. Biosci Rep. 2018;38(3). https://doi.org/10.1042/BSR20180289.